Journal of Materials Chemistry A

PAPER

View Article Online
View Journal | View Issue

Cite this: J. Mater. Chem. A, 2014, 2, 15788

An epidermal alkaline rechargeable Ag–Zn printable tattoo battery for wearable electronics†

Sheela Berchmans,[ab] Amay J. Bandodkar,[a] Wenzhao Jia,[a] Julian Ramírez,[a] Ying S. Meng*[a] and Joseph Wang*[a]

Received 25th June 2014
Accepted 18th July 2014

DOI: 10.1039/c4ta03256j

www.rsc.org/MaterialsA

Herein we report for the first time the fabrication of a rechargeable, benign, skin-worn Ag–Zn tattoo battery using unconventional materials, such as screen printed electrodes, temporary tattoo paper, alkaline gel electrolytes and a PDMS cover for sealing the battery. The tattoo battery can be easily worn by a person for powering wearable devices. Detailed characterization of a typical Ag–Zn tattoo cell reveals a capacity density in the range 1.3–2.1 mA h cm^{-2} and stability up to 13 cycles. The tattoo cell exhibits a stable open circuit voltage of 1.5 V over a 5 days period and endures repeated stretching and bending strain cycles with minimal decrement in its performance. The lateral arrangement of the negative and positive electrodes allows the integration of several cells into a battery in series or parallel combination for tuning the discharge capacity and voltage to the desired values. The practical nature of the tattoo battery was illustrated by applying it to a human subject's skin followed by lighting a red LED. The epidermal tattoo battery thus meets the demands of wearable power sources, including mechanical compliance and tunable discharge capacity, to power body-worn electronic devices.

Introduction

The development of wearable health systems has made considerable progress in recent years. The advent of wearable electronics and wireless networks have facilitated the real-time on-body monitoring of vital physical signs,[1] such as blood pressure, heart rate, or skin temperature, as well as of chemical parameters like lactate,[2] pH[3] and sodium.[4] However, powering such on-body sensors is a challenging problem which can be addressed by self-powered devices or by wearable power sources. Recent efforts have led to innovative solutions such as flexible thin-film batteries,[5,6] piezoelectric nanogenerators,[7] wearable solar cells,[8,9] microsupercapacitors,[10] wearable thermoelectric generator,[11] epidermal biofuel cells[12] and endocochlear-potential-based biobatteries.[13] Of these, thin-film wearable batteries hold the highest promise as they can provide high power levels at low cost and can be recharged for repeated use. Despite of their tremendous potential, much needs to be achieved in the wearable battery field to keep pace with the rapidly growing field of wearable and implantable devices. Merger of materials science and energy technology can ultimately lead to the development of ultrathin, safe energy storage devices that can be easily incorporated on to clothes, eye glasses, wrist watches, and even skin to power modern wearable gadgets.[14]

Lack of compliant rechargeable wearable batteries that conform well to the contours of the body is a major bottleneck in the development of wearable electronics. Conventional batteries consist of rigid metallic substrates and thus cannot be directly used as wearable skin-worn power sources. The main components of the battery, *viz.*, electrode, separator and electrolyte, thus need to be modified for enduring complex body movements without compromising the battery's performance. Construction of energy devices based on unconventional substrates, such as polymer films, metal foils, paper, textile or rubber slabs, is becoming popular as indicated from the current literature. Particular attention has been given to the development of flexible Li ion batteries due to their high open circuit voltage, high energy density, low self-discharge and lack of memory effect. Different versions of the flexible Li battery, such as stretchable battery with serpentine interconnects withstanding 300% stretchability,[15] wearable textile-based Li battery,[16] paper-based origami Li battery,[17] CNT and CNT composite based Li batteries on paper supports[18,19] and cable type Li batteries,[20] have been reported in the literature. Dry batteries (Zn–carbon, Leclanche batteries), on the other hand, are considered as economic and environmental friendly. Compliant versions of dry batteries have been reported with electrospun carbon mats as cathode, along with Zn foil anode in the presence of polyethylene oxide (PEO) electrolyte containing TiO_2 nanoparticles[21] and also with stretchable carbon-paste

[a]Department of Nanoengineering, University of California San Diego, 9500 Gilman Drive, La Jolla, CA 92093, USA. E-mail: josephwang@ucsd.edu; shirleymeng@ucsd.edu

[b]EEC Division (Biosensors Group), CSIR-Central Electrochemical Research Institute, Karaikudi, 63006, Tamilnadu, India

† Electronic supplementary information (ESI) available. See DOI: 10.1039/c4ta03256j

based current collectors where a Zn paste (made of Zn, carbon black and xanthan gel) served as anode and MnO_2 paste (made of MnO_2, carbon black and electrolyte paste) acting as cathode.[22] Alkaline batteries are similar to dry batteries and flexible versions of such systems have been fabricated using conductive textile substrates for wearable applications.[5,23–25] Ag–Zn batteries are being used in small and large scale applications. A stretchable Ag–Zn battery based on embedded nanowire elastic conductors was recently reported.[26] However, they can provide a maximum areal capacity of only 0.11 mA h cm^{-2} due to the low areal density of nanowire configuration. Other type of battery systems, such as Zn–air,[27] Al–Cu[28,29] and Mg–Cu[30,31] based on paper supports, have also been reported. Some of the paper-based battery systems have been integrated into microfluidic channels and microelectrochemical sensing platforms for the development of self-powered analytical systems.[32–36]

The present article reports on the fabrication and characterization of an epidermal tattoo-based Ag–Zn rechargeable battery for powering wearable electronics. Ag–Zn batteries belong to a class of mature battery systems that provide high power and are preferred for critical large scale applications in space, underwater and military as well as on smaller scale, for example, powering watches. Ag–Zn cells are safer as they make use of the water-based electrolytes, unlike Li-ion batteries which rely on hazardous nonaqueous solvents. Zinc-based batteries also provide an attractive alternative to Li-ion batteries because of the extensive global reserves of Zn. Hence, Ag–Zn cells represent an attractive choice for use in wearable, flexible devices. Though, silver is relatively expensive, the virtues of an Ag–Zn galvanic cell, namely, lower toxicity, ability to work without glove-box and possibility to develop all-printed batteries make it a better choice for wearable applications as compared to its Li counterparts. The new skin-worn Ag–Zn tattoo cell, inspired by our earlier work on tattoo-based electrochemical sensors,[3,4] has been realized by amalgamating diverse screen printing, temporary tattoo and thin-film battery technologies (Fig. 1). The tattoo battery is referred to as an "epidermal" device since it adheres directly to the epidermis (outermost layer of the human skin) similar to a commercial temporary tattoo. As these devices can be applied directly to the skin, they offer great levels of freedom to the wearer for applying them to any location on the skin. Such freedom is not feasible in case of plastic and textile-based battery devices. Additionally, the tattoo batteries are fabricated using inexpensive screen printing technology which lowers the device cost significantly. The versatility of the printing technology offers great freedom to develop tattoo-based batteries of any shape and allows several cells to be connected in parallel and/or series combination to alter the total voltage and current. Tattoo papers are also relatively cheap, thin, light weight, flexible, biocompatible and biodegradable.

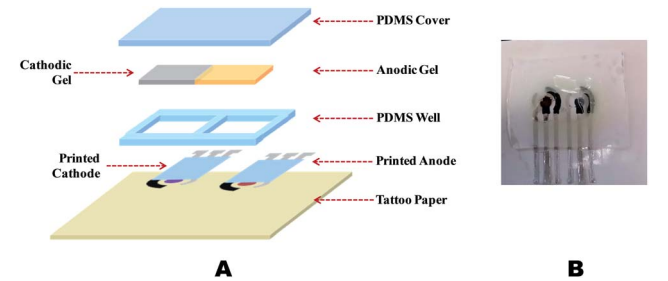

Fig. 1 (A) Schematic diagram illustrating the different steps involved in the fabrication of the Ag–Zn cell. (B) The prototype of the Ag–Zn cell on temporary transfer tattoo support.

Experimental

Materials

The following chemicals were used as received without further purification: $ZnSO_4$ (Fluka), H_3BO_3 (EMD), sulphuric acid (EMD), Ag plating solution (Technic Inc. Rhode Island), KOH (Sigma-Aldrich), LiOH (Sigma-Aldrich), poly acrylic acid (Sigma-Aldrich), poly acrylic acid-partial potassium salt (Sigma-Aldrich), ZnO (Sigma-Aldrich).

Fabrication of Ag–Zn cell

A typical Ag–Zn tattoo cell was constructed using inkjet tattoo paper (Papilio, HPS LLC, Rhome, TX) as support. Electrode patterns were designed in AutoCAD (Autodesk, San Rafael, CA) and outsourced for fabrication on stainless steel through-hole 12 inch framed stencils (Metal Etch Services, San Marcos, CA). A sequence of the transparent insulator (DuPont 5036 Wilmington, DE), Ag layer (Dupont 5874, Wilmington, DE) as reference electrode, carbon layer (E3449, Ercon, Inc., Wareham, MA) as current collector followed by a final layer of transparent insulator for defining electrode active area was screen printed employing an MPM-SPM semiautomatic screen printer (Speedline Technologies, Franklin, MA). Three electrode configuration facilitates electrodeposition of the active materials Zn (negative electrode) and Ag (positive electrode) separated by 1 cm. A pair of three electrodes was printed laterally on a tattoo paper which provides scope for integrating arrays of cells into a battery. The electrochemical experiments were performed using microAutolab type III (Metrohm, the Netherlands). Ag and Zn were electrodeposited on the active carbon area ($\phi = 3$ mm) at a current density of -1.75 mA for 600 s using plating solutions of Ag and Zn respectively. The composition of the Zn plating solution is as follows: 80 g l^{-1} $ZnSO_4$, and 20 g l^{-1} H_3BO_3 solutions (buffered to pH = 2.5 with sulfuric acid). After electrodeposition the counter and reference electrodes were masked by a thin film of epoxy and two wells of epoxy were created around the Ag and Zn electrodes which were then filled with poly acrylic acid gel electrolytes. The Ag electrode was covered with gel containing 3% poly acrylic acid (PAA) containing 6 M KOH + 1 M LiOH. The Zn electrode was covered with a gel containing 10% poly acrylic acid partial potassium salt (PAA-K) containing 6 M KOH + 1 M LiOH saturated with ZnO. The gap between the electrode wells was covered with the gel containing 3% poly acrylic acid (PAA) containing 6 M KOH + 1 M LiOH which provides the required ionic contact between the

anode and cathode compartments. The electrodes surrounded by the gel was subsequently covered with a PDMS film and sealed with epoxy glue. The casting solution was prepared by mixing PDMS prepolymer and the initiator from the Sylgard 184 silicone elastomer kit in the 10 : 1 ratio followed by curing at 90 °C for 10 min. The film of the required thickness was obtained by casting the solution on a glass plate. The final thickness of the device was approximately 2 mm. The tattoo battery was transferred to receiving substrates (Gore-tex® fabric or human skin) in a manner discussed in our earlier work.[2,3] Prior to the on-body test, consent was obtained from the human subject. The test was performed in compliance with the protocol that was approved by the institutional review board (IRB) at the University of California, San Diego. It should be pointed out that the release agent-coated tattoo base paper is used as a support to fabricate the entire tattoo battery. The tattoo battery transfer process involved applying a thin layer of transparent adhesive to the device, followed by its adherence to the receiving substrate. Finally, the tattoo paper was gently removed by dabbing the paper with water.

Electrochemical measurements

Charge–discharge studies of the Ag–Zn tattoo cell were carried out galvanostatically (microAutolab type III, Metrohm, the Netherlands) by applying a current of 100 μA or 150 μA. The charge–discharge cycles were carried out in the voltage range 2.05 V to 0.8 V. Between each cycle an interval of 10 minutes was given during which open circuit voltage (OCV) of the cell was monitored. Electrochemical impedance measurements were carried out using CH instrument electrochemical analyser (CHI 660D CH Instruments, Austin, TX) in the frequency region 0.1 Hz to 1 MHz at an AC amplitude of 10 mV. The measurements were recorded at the open circuit voltage of the cell.

Mechanical testing

The mechanical resiliency of the tattoo cell was examined by subjecting the cell to repeated bending and stretching after transferring the cell to a stretchable Gore-tex® fabric. In the case of stretching study, the tattoo cell was stretched along the length of the electrodes at a controlled speed of 0.1 mm s^{-1} and an increasing strain from 0 to 11.1% was applied to the tattoo cell using a tensile test machine (Instron® 5900 Series Model 5982, Norwood, MA). The effect of mechanical deformations was monitored by discharge using linear polarisation measurements between the voltage limits 2.05 V and 0.8 V at a scan rate of 2 mV s^{-1} and by galvanostatic discharge method. The discharge test using linear polarisation was performed after every 5 fatigue cycles for a total of 25 cycles. The bending study comprised of subjecting the tattoo cell to a bending stress of 180° along the latitude. The tattoo cell was repeatedly bent perpendicular to the length of the electrodes for a total of 100 fatigue cycles and the discharge data using linear polarisation was recorded after every 20 bending iterations. A galvanostatic discharge was carried out at the completion of all the fatigue cycles during stretching and bending.

SEM

Scanning electron microscopy (SEM) images were taken using a Phillips XL30 ESEM instrument with an acceleration potential of 20 kV. All SEM samples were sputtered with iridium for 7 s before imaging. SEM images were recorded for the electrodeposited positive and negative electrodes (Ag and Zn electrodes on carbon collectors) and also for the positive and the negative electrodes removed from the cell after complete discharge.

Results and discussion

Redox reactions at the negative and positive electrodes

Fig. 2A shows the typical redox reactions of the Ag–Zn tattoo cell and the cyclic voltammograms corresponding to the negative (Zn) and the positive (Ag) electrodes. The cyclic voltammograms shown in Fig. 2B and C represent the electrochemical response of the negative and positive electrodes in 6 M KOH + 1 M LiOH electrolyte at a scan rate of 5 mV s^{-1}. The response of the negative electrode shows the redox behaviour of the Zn electrode constituting of the $Zn/Zn(OH)_2$ redox couple. The redox reaction is quasi reversible as seen from the voltammogram. The response of the positive electrode corresponds to the formation of the two oxides, Ag_2O and AgO (Fig. 2C). The redox couples that exist at the positive electrode are AgO/Ag_2O and Ag_2O/Ag. Thus, the reduction of AgO to Ag occurs in two stages. The Ag_2O/Ag redox couple is reversible and the redox couple AgO/Ag is quasi reversible as seen from the voltammogram:

$$Ag_2O + H_2O + 2e^- \underset{\text{Charge}}{\overset{\text{Discharge}}{\rightleftharpoons}} 2Ag + 2OH^- \quad E^o = 0.34 \text{ V } \textit{vs.} \text{ SHE} \tag{1}$$

$$2AgO + H_2O + 2e^- \underset{\text{Charge}}{\overset{\text{Discharge}}{\rightleftharpoons}} Ag_2O + 2OH^- \quad E^o = 0.6 \text{ V } \textit{vs.} \text{ SHE} \tag{2}$$

Discharge characteristics of the Ag–Zn tattoo cell

The discharge characteristics of a typical Ag–Zn tattoo cell are shown in Fig. 3(A–C). The Ag–Zn tattoo cell was subjected to galvanostatic charge–discharge cycling in the voltage limits between 2.05 and 0.8 V at the rate of 1.4 mA cm^{-2}. The variation of cell voltage during a charge–discharge cycle is illustrated in Fig. 3A. The two plateau regions at 1.7 and 2.0 V observed during charging correspond to the two stages of oxidation of the positive electrode (reactions (1) and (2), respectively). The sharp rise observed during charging corresponds to the formation of high resistance Ag_2O layer and the formation of the second plateau corresponds to the formation of AgO.[37] The voltage spike observed between the first and the second plateau is due to highly resistive Ag_2O completely surrounding the electrode. Upon complete charging the sudden sharp voltage rise is attributed to the electrolysis of water. During discharge, there is a gradual decrease of the voltage from 1.8 to 1.5 V. The voltage remains fairly constant at 1.5 V for major section of discharging followed by a rapid decrease at the end. The gradual decrease of

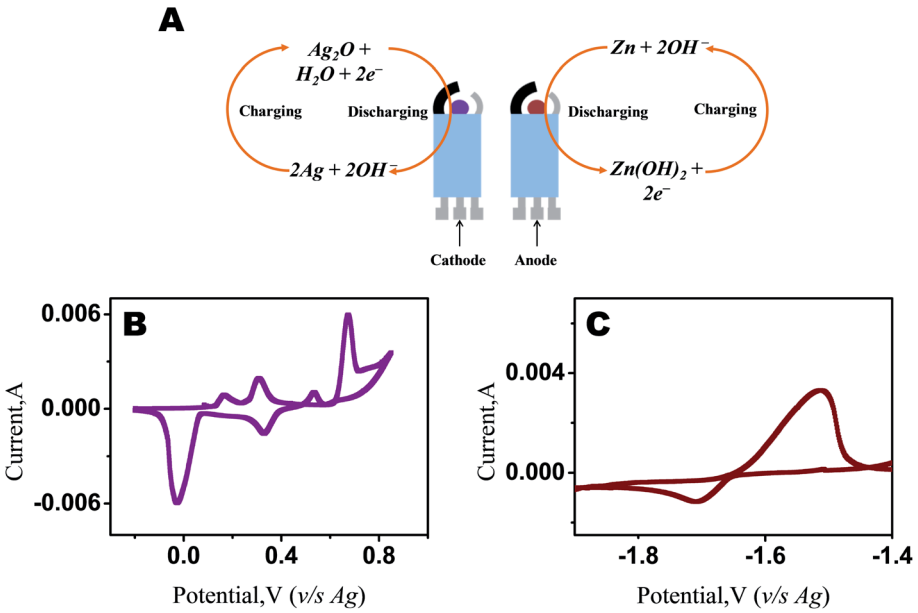

Fig. 2 (A) Typical redox reactions at the negative and positive electrodes. (B) Cyclic voltammetric response of the positive Ag electrode. (C) Cyclic voltammetric response of the negative Zn electrode in 6 M KOH + 1 M LiOH at 5 mV s^{-1}.

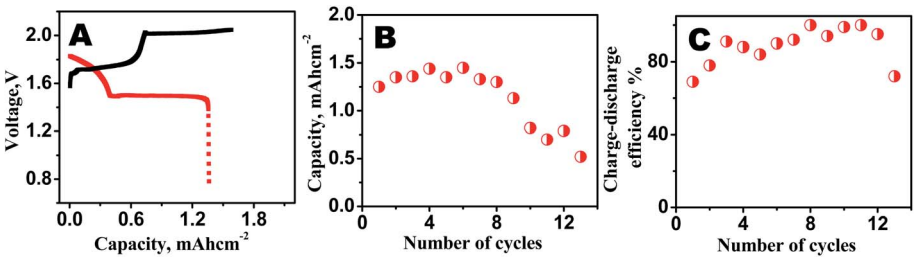

Fig. 3 (A) Typical charge–discharge characteristic of an Ag–Zn tattoo cell. (B) Discharge capacity *vs.* number of cycles. (C) Charge–discharge efficiency *vs.* number of cycles.

voltage from 1.8 to 1.5 V is due to the first-stage reduction of AgO to Ag_2O (reaction (2)), wherein these two compounds form a solid solution. The decrease in voltage is due to an increase in concentration of Ag_2O in the AgO–Ag_2O solid solution. The second discharge-plateau at 1.5 V is due to the constant concentration of $Ag(OH)_2$. The potential of the negative electrode, namely $Zn/Zn(OH)_2$ is expected to be constant throughout the discharge due to the constant concentration of supersaturated $Zn(OH)_4^{2-}$ ions.

The discharge capacity over 13 cycles is shown in Fig. 3B. An average discharge capacity of 1.48 mA h cm^{-2} is observed over 8 cycles. Thereafter, the capacity starts decreasing and reaches a value of 0.5 mA h cm^{-2} at the 13th cycle. The charge–discharge efficiency is shown in Fig. 3C. The efficiency increases from 69% for the first cycle and remains close to 90% up to 12 cycles and finally goes down to 72%. A maximum volumetric capacity of 2.94 mA h cm^{-3} was achieved. However, the cycling ability of the cell decreases when the cell is discharged at higher rates (for example: 2.14 mA h cm^{-2}) (see ESI, Fig. S1†). The charge–discharge efficiency of the cell can be improved by suppressing hydrogen evolution at the anode, improving the electrochemical reversibility and stability of silver oxides and further optimizing the battery fabrication and sealing process. It can be shown that the power output of the tattoo cell can be improved by printing three current collectors to build a cell with an Ag–Zn–Ag configuration. The discharge capacity of such a cell was found to be 2.1 mA h cm^{-2} (see ESI, Fig. S2†). This indicates that arrays of the cell can be designed by lateral printing of current collectors on a tattoo paper and integrate them into a battery depending upon the specific power requirements. The OCV of the Ag–Zn tattoo cells were stable at 1.5 V and the life of the cell was around 3–5 days (ESI, Fig. S3†).

Effect of mechanical deformations

A wearable device must conform perfectly to the human body and show minimal effect on its performance due to the mechanical deformations experienced by the skin during ambulatory activities of the body. A temporary tattoo based device adheres well to the complex morphology of the human epidermis and can survive for long durations.[38] The mechanical resiliency of the tattoo battery was examined by subjecting it to

repeated bending and stretching iterations that mimic the mechanical stress usually endured by the human epidermis.

Stretching effect. The effect of stretching stress on tattoo battery performance was evaluated by applying the tattoo battery to Gore-tex® and subjecting it to increasing levels of tensile strain. The discharge characteristics of the tattoo cell was measured after every 5 stretching fatigue cycles by linearly varying the voltage from 2.05 V to 0.8 V at 2 mV s^{-1} (Fig. 4A). The peak current corresponding to the reduction of Ag_2O to Ag decreases from 27 mA cm^{-2} to 6 mA cm^{-2} upon increasing the strain to 11.1%. At the end of stretching experiments a galvanostatic discharge was finally conducted to check the performance of the cell. After the stretching experiments the galvanostatic discharge capacity decreased to 18% of the initial discharge capacity (Fig. 4B and C).

Bending effect. The human epidermis regularly undergoes stress generated due to bending of muscles. The effect of such bending stress was analysed on the tattoo battery by bending it by 180° along the latitude for up to 100 times. Similar to the stretching study, the discharge characteristics of the tattoo battery was measured after every 20 bending cycles by linearly varying the voltage from 2.05 V to 0.8 V at a scan rate of 2 mV s^{-1}. As seen from the figure, the changes in the peak current due to reduction of Ag_2O to Ag can be ascribed to the effect of bending. After 100 bendings the current density of the Ag_2O/Ag peak decreased from an initial value of 20 mA cm^{-2} to 14.5 mA cm^{-2} (Fig. 5A) and the galvanostatic discharge capacity decreased to 66% (Fig. 5B and C). The study thus reveals the resiliency of the tattoo cell to withstand large number of bending fatigue cycles with minimal effect on its performance. The effect of bending stress was also monitored by coupling 2 Ag–Zn tattoo cells in series to light up a red LED (operating voltage 1.8 V; current consumption 20 mA). Fig. 5D and E clearly demonstrate that the tattoo battery can perform very well even under extreme deformation conditions, underscoring the practical nature of the wearable tattoo battery system. (This study was performed after removal of the tattoo base paper.) It was observed that the tattoo device adhered firmly to the underlying Gore-tex® substrate even after it was subjected to repeated bending and stretching stressors. This observation emphasizes that the tattoo battery can withstand the deformations expected during real-life use of such devices.

Morphology of the electrodes

SEM images of the active materials are presented in Fig. 6. For example, Fig. 6A and B displays SEM images of the

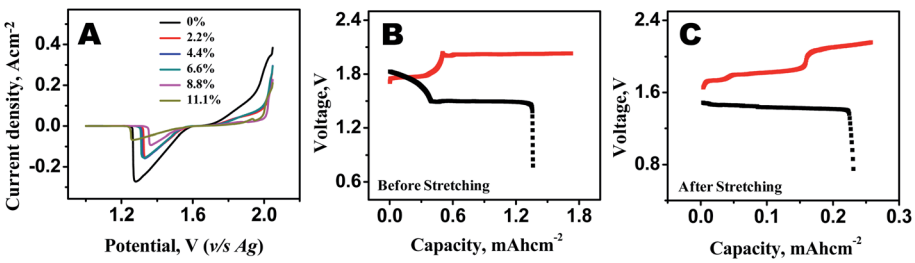

Fig. 4 (A) Linear sweep discharge curves at 2 mV s^{-1} for different percentages of stretching. (B) Galvanostatic charge–discharge before discharge experiments. (C) Galvanostatic charge–discharge after stretching experiments. Red plot corresponds to the charging curve while black plot corresponds to the discharge curve in figures (B) and (C).

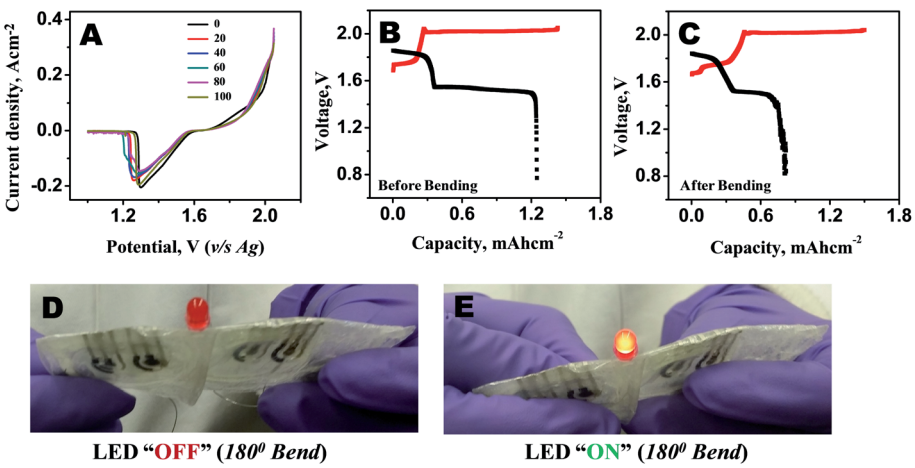

Fig. 5 (A) Linear sweep discharge curves at 2 mV s^{-1} recorded over 5 bend cycles. (B) Galvanostatic discharge before bending. (C) Galvanostatic discharge after bending. (D, E) Demonstration of the performance of the tattoo battery under deformed conditions. Red plot corresponds to the charging curve while the black plot corresponds to the discharge curve in figures (B) and (C).

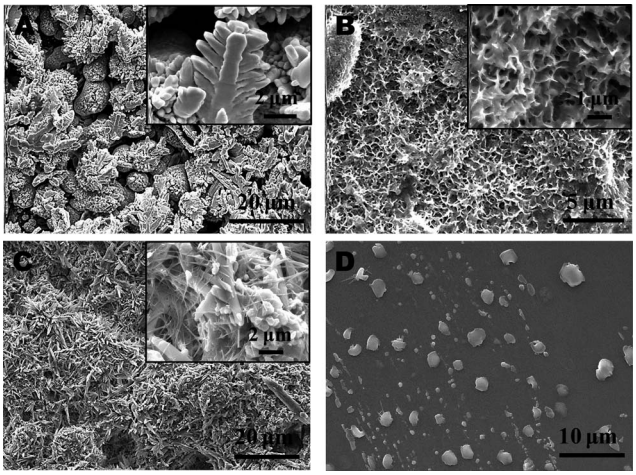

Fig. 6 SEM images of (A) electrodeposited Ag electrode on carbon current collector (inset: zoomed in image of the Ag electrode). (B) Electrodeposited Zn electrode on carbon current electrode (inset: zoomed in image of the Zn electrode). (C) Ag electrode after complete discharge (inset: zoomed in image of the Ag electrode). (D) Zn electrode after discharge.

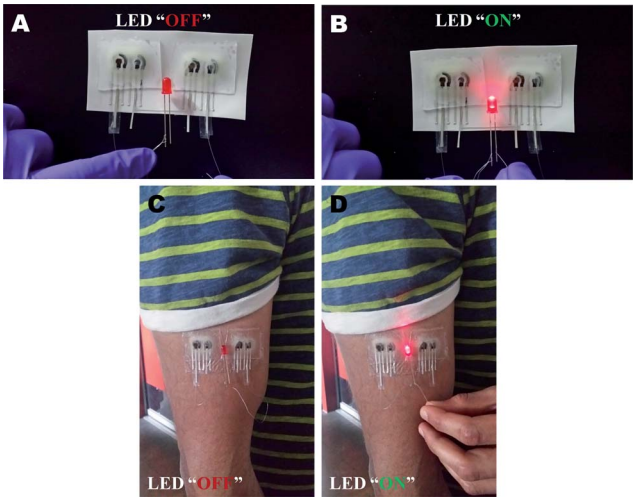

Fig. 7 Demonstration of practical utility of the tattoo battery for lighting a red LED (A and B) before transfer onto skin (C and D) after transfer onto skin.

electrodeposited Ag and Zn active materials, respectively, on the carbon current collector. The electrodeposited Ag electrode has a clustered nano-dendritic structure while the SEM image of Zn electrode reveals a nano-porous morphology. SEM analysis was also performed after complete discharge of the Ag–Zn cell. The effect of complete discharge on both the electrodes can be easily observed *via* the SEM images (Fig. 6C and D). After complete discharge the morphology of the Ag electrode transforms to nanowires and flakes from the nano-dendritic structure (Fig. 6C). This may be due to the presence of a mixture of several active components (Ag, Ag_2O and AgO) on the positive electrode. On the other hand, the electrodeposited Zn on the negative electrode dissolves during the discharge process, leading to the loss of the nano-porous structure (Fig. 6D).

On body transfer of the tattoo battery

This section demonstrates the epidermal application of the new tattoo battery in real-life scenarios. In this study, two tattoo cells were connected in series to power a LED. A consenting human subjected to apply the tattoo battery to his right deltoid. The tattoo transfer process is similar to our earlier reported works.[2,3] The tattoo battery was easily worn by the subject without any assistance. Upon transfer of the tattoo battery, a red LED (operating voltage 1.8 V; current consumption 20 mA) was turned 'ON' by connecting it in series with the skin-worn tattoo battery. Fig. 7A and B illustrate the tattoo battery in action, lighting a LED before transfer onto the skin. Fig. 7C and D show photograph of the tattoo battery transferred on to the human subject in "ON" and "OFF" states. The study demonstrates the pragmatic nature of the developed tattoo-based alkaline batteries to power devices. The epidermal tattoo batteries can be removed from the skin and applied back by using a fresh transparent adhesive for repeated use.

Performance analysis

Literature reveals that there is quite a lot of interesting investigations going on with the development of flexible Li-ion batteries.[15–20] Li-ion batteries face major challenging issues due to the flammability of the organic electrolyte, and the reactivity of the electrode materials with the organic electrolytes in case of improper use such as overcharging or short-circuiting. Alkaline Ag–Zn batteries with discharge current density of 1.8 mA cm^{-2} have been reported.[39] However, the rigid gold sputtered glass substrate utilized for the fabrication of these batteries limit their use for wearable applications. Recent work on stretchable Ag–Zn batteries addresses the issue body compliance.[26] However, the battery reveals a low discharge capacity of 0.11 mA h cm^{-2}. Though the paper reports 1000 charging cycles, the study was performed for the silver electrode and not for the entire battery system. Similarly, a fabric-based Ni–Zn battery using microfiber substrate and separator with an areal capacity of 1.4 μA h cm^{-2} after four discharge cycles, has also been reported.[40] The present work describes a novel method to power skin electronics by building Ag–Zn batteries on temporary transfer tattoo supports. The resulting flexible tattoo-based Ag–Zn battery has a discharge capacity of 2.1 mA h cm^{-2} for 13 cycles and can endure repeated mechanical stress. Thus, the tattoo battery meets the demands of wearable electronics, offering attractive flexibility and good discharge capacity. Ag–Zn cells are less toxic and the alkaline electrolyte used in this work has been used in prior work for developing medical devices.[41] The new tattoo battery displays limiting cycling capabilities and relatively higher internal resistance, reflected by the electrochemical impedance analysis of the battery (see ESI, Fig. S4†). The capacity losses could arise during the fabrication process, use of gel electrolytes and due to the formation of resistive Ag_2O species at the positive electrode. The morphology changes of the anode and cathode after complete discharge also explains the capacity loss during cycling. Hydrogen evolution occurring at the negative electrode could be another reason for the capacity loss.

Conclusions

We have demonstrated the fabrication and operation of a non-toxic printable Ag–Zn tattoo battery that can be easily worn onto the skin to power wearable electronics. The work provides, for the first time, insights in the fabrication on printed wearable batteries using cost-effective screen printing and temporary tattoo technologies. The battery can be transferred onto body without the need of a special casing for the battery. The inexpensive tattoo paper aids the translation of conventional battery to a wearable design. The lateral disposition of the anode and cathode allows us to build the battery in arrays and to tune the power requirements at our will. The epidermal battery is rechargeable and its flexibility is demonstrated by repeated stretching and bending experiments. The performance of the tattoo battery (resiliency towards stretching stress, charge–discharging efficiency, *etc.*) may be enhanced by further improving the design parameters including electrode architecture and types of electrolytes. This represents an important step towards building rechargeable batteries on temporary transfer tattoos for facile transfer to the skin ushering us towards "tattoo-tronics" for flexible electronics.

Acknowledgements

This project was supported by National Science Foundation (Awards CBET-1066531). SB acknowledges USIEF for Fulbright-Nehru senior research fellowship and the Director Central Electrochemical Research Institute, Karaikudi, India, for sanctioning leave to avail the fellowship. Y. S. Meng acknolwdges the Qualcomm gift fund. We thank S. Sattayasamitsathit and X. Wang for recording SEM images and preparation of reagents respectively.

References

1 D. H. Kim, R. Ghaffari, N. Lu and J. A. Rogers, *Annu. Rev. Biomed. Eng.*, 2012, **14**, 113–128.
2 W. Jia, A. J. Bandodkar, G. Valdés-Ramírez, J. R. Windmiller, Z. Yang, J. Ramírez, G. Chan and J. Wang, *Anal. Chem.*, 2013, **85**, 6553–6560.
3 A. J. Bandodkar, V. W. S. Hung, W. Jia, G. Valdes-Ramírez, J. R. Windmiller, A. G. Martinez, J. Ramírez, G. Chan, K. Kerman and J. Wang, *Analyst*, 2013, **138**, 123–128.
4 A. J. Bandodkar, D. Molinnus, O. Mirza, T. Guinovart, J. R. Windmiller, G. Valdés-Ramírez, F. J. Andrade, M. J. Schöning and J. Wang, *Biosens. Bioelectron.*, 2014, **54**, 603–609.
5 A. M. Gaikwad, G. L. Whiting, D. A. Steingart and A. C. Arias, *Adv. Mater.*, 2011, **23**, 3251.
6 C. Yan and P. S. Lee, *Small*, 2014, DOI: 10.1002/smll.201302806.
7 Y. Qin, X. D. Wang and Z. L. Wang, *Nature*, 2008, **451**, 809–813.
8 L. H. Zhang, E. Z. Shi, C. Y. Ji, Z. Li, P. X. Li, Y. Y. Shang, Y. B. Li, J. Q. Wei, K. L. Wang, H. W. Zhu, D. H. Wu and A. Y. Cao, *Nanoscale*, 2012, **4**, 4954–4959.
9 S. Zhang, C. Ji, Z. Bian, R. Liu, X. Xia, D. Yun, L. Zhang, C. Huang and A. Cao, *Nano Lett.*, 2011, **11**, 3383–3387.
10 J. Bae, M. K. Song, Y. J. Park, J. M. Kim, M. L. Liu and Z. L. Wang, *Angew. Chem., Int. Ed.*, 2011, **50**, 1683–1687.
11 S. J. Kim, J. H. We and B. J. Cho, *Energy Environ. Sci.*, 2014, **7**, 1959–1965.
12 W. Jia, G. Valdés-Ramírez, A. J. Bandodkar, J. R. Windmiller and J. Wang, *Angew. Chem., Int. Ed.*, 2013, **52**, 7233–7236.
13 P. P. Mercier, A. C. Lysaght, S. Bandyopadhyay, A. P. Chandrakasan and K. M. Stankovic, *Nat. Biotechnol.*, 2012, **30**, 1240–1243.
14 D. H. Kim, N. Lu, R. Ma, Y. S. Kim, R. H. Kim, S. Wang, J. Wu, S. M. Won, H. Tao, A. Islam, K. J. Yu, T. Kim, R. Chowdhury, M. Ying, L. Xu, M. Li, H. J. Chung, H. Keum, M. McCormick, P. Liu, Y. W. Zhang, F. G. Omenetto, Y. Huang, T. Coleman and J. A. Rogers, *Science*, 2011, **333**, 838–843.
15 S. Xu, Y. Zhang, J. Cho, J. Lee, X. Huang, L. Jia, J. A. Fan, Y. Su, J. Su, H. Zhang, H. Cheng, B. Lu, C. Yu, C. Chuang, T. Kim, T. Song, K. Shigeta, S. Kang, C. Dagdeviren, I. Petrov, P. V. Braun, Y. Huang, U. Paik and J. A. Rogers, *Nat. Commun.*, 2013, **4**, 1–8.
16 Y. H. Lee, J. S. Kim, J. Noh, I. Lee, H. Jun Kim, S. Choi, J. Seo, S. Jeon, T. S. Kim, J. Y. Lee and J. W. Choi, *Nano Lett.*, 2013, **13**, 5753–5761.
17 Z. Song, T. Ma, R. Tang, Q. Cheng, X. Wang, D. Krishnaraju, R. Panat, C. K. Chan, H. Yu and H. Jiang, *Nat. Commun.*, 2014, **5**, 3140.
18 L. Hu, H. Wu, F. L. Mantia, Y. Yang and Y. Cui, *ACS Nano*, 2010, **4**, 5843–5848.
19 V. L. Pushparaj, M. M. Shaijumon, A. Kumar, S. Murugesan, L. Ci, R. Vajtai, R. J. Linhardt, O. Nalamasu and P. M. Ajayan, *Proc. Natl. Acad. Sci. U. S. A.*, 2007, **104**, 13574–13577.
20 Y. H. Kwon, S.-W. Woo, H. R. Jung, H. K. Yu, K. Kim, B. H. Oh, S. Ahn, S. Y. Lee, S. W. Song, J. Cho, H. C. Shin and J. Y. Kim, *Adv. Mater.*, 2012, **24**, 5192–5197.
21 P. Hiralal, S. Imaizumi, H. E. Unalan, H. Matsumoto, M. Minagawa, M. Rouvala, A. Tanioka and G. A. J. Amaratunga, *ACS Nano*, 2010, **4**, 2730–2734.
22 M. Kaltenbrunner, G. Kettlgruber, C. Siket, R. Schwödiauer and S. Bauer, *Adv. Mater.*, 2010, **22**, 2065–2067.
23 A. M. Gaikwad, D. A. Steingart, T. N. Ng, D. E. Schwartz and G. L. Whiting, *Appl. Phys. Lett.*, 2013, **102**, 233302–233306.
24 A. M. Gaikwad, H. N. Chu, R. Qeraj, A. M. Zamarayeva and D. A. Steingart, *Energy Technol.*, 2013, **1**, 177–185.
25 G. Kettlgruber, M. Kaltenbrunner, C. M. Siket, R. Moser, I. M. Graz, R. Schwödiauer and S. Bauer, *J. Mater. Chem. A*, 2013, **1**, 5505–5508.
26 C. Yan, X. Wang, M. Cui, J. Wang, W. Kang, C. Y. Foo and P. S. Lee, *Adv. Energy Mater.*, 2014, **4**, 1301396.
27 M. Hilder, B. Winther-Jensen and N. B. Clark, *J. Power Sources*, 2009, **194**, 1135–1141.
28 I. Ferreira, B. Brás, N. Correia, P. Barquinha, E. Fortunato and R. Martins, *J. Disp. Technol.*, 2010, **6**, 332–335.
29 I. Ferreira, B. Brás, J. I. Martins, N. Correia, P. Barquinha, E. Fortunato and R. Martins, *Electrochim. Acta*, 2011, **56**, 1099–1105.
30 K. B. Lee, *J. Micromech. Microeng.*, 2005, **15**, S210–S214.

31 K. B. Lee, *J. Micromech. Microeng.*, 2006, **16**, 2312–2317.
32 N. K. Thom, K. Yeung, M. B. Phillion and S. T. Phillips, *Lab Chip*, 2012, **12**, 1768–1770.
33 N. K. Thom, G. G. Lewis, M. J. Di Tucci and S. T. Phillips, *RSC Adv.*, 2013, **3**, 6888–6895.
34 X. Zhang, J. Li, C. Chen, B. Lou, L. Zhang and E. Wang, *Chem. Commun.*, 2013, **49**, 3866–3868.
35 X. Zhang, Z. Lin, B. Chen, S. Sharma, C. Wong and Y. Deng, *J. Mater. Chem. A*, 2013, **1**, 5835–5839.
36 H. Liu and R. M. Crooks, *Anal. Chem.*, 2012, **84**, 2528–2532.
37 P. Suresh, D. H. Nagaraju, A. K. Shukla and N. Munichandraiah, *Electrochim. Acta*, 2005, **50**, 3262–3272.
38 J. R. Windmiller, A. J. Bandodkar, G. Valdés-Ramírez, S. Parkhomovsky, A. G. Martinez and J. Wang, *Chem. Commun.*, 2012, **48**, 6794–6796.
39 K. T. Braam, S. K. Volkman and V. Subramanian, *J. Power Sources*, 2012, **199**, 367–372.
40 J. K. Kim, A. Armutlulu, M. Kim, S. Paik, S. A. B. Allen and M. G. Allen, *Power MEMS*, 2012, 371–374.
41 D. Coates, E. Ferreira and A. Charkey, *J. Power Sources*, 1997, **65**, 109–115.